Synthesizing Circularly Polarized Multi-beam Planar Dipole Arrays with Sidelobe and Cross-Polarization Control by Two-Step Element Rotation and Phase Optimization

Yang Peng, Yanhui Liu, *Senior Member, IEEE*, Ming Li, Haiwen Liu, *Senior Member, IEEE*, and Y. Jay Guo *Fellow, IEEE*

***Abstract*—In this paper, a novel method is presented to synthesize multi-beam circularly polarized (CP) patterns with sidelobe level (SLL) and cross-polarization level (XPL) suppression for planar dipole arrays by optimizing both element rotations and excitation phases. Multiple sets of excitation phases are adopted as optimization variables other than the determined values according to the rotation angles in the conventional sequentially rotated technique (SRT) and the random sequentially rotated technique (RSRT), so as to improve the performance of the obtained CP multi-beam patterns. This releases many more degrees of synthesis freedom but leads to a new problem of demanding excessive computation resources for a planar rotated dipole array with multiple CP patterns. Then, a two-step rotation and phase optimization strategy is proposed to effectively solve this optimization problem. In its initial step, the common element rotations and approximated excitation phases composed of the common phase parts plus the beam focusing phase parts are found for multiple desired CP patterns with different beam directions. And then, a refining step is performed to refine the excitation phases individually for each CP beam for improved pattern performance. Four representative examples of synthesizing multi-beam patterns with both SLL and XPL suppression are provided to verify the effectiveness of the proposed method. Comparisons with the conventional SRT and RSRT are also provided to show the superiority of the proposed method.**

***Index Terms*—Circularly polarized multi-beam patterns, element rotation and phase optimization, two-step optimization strategy, planar rotated dipole array.**

I. Introduction

ANTENNA arrays radiating circular polarization (CP) beam patterns have been widely used in many applications such as satellite communications [1], [2], global positioning systems [3], [4], and some high-performance radars [5], [6], since the systems working in the CP wave propagation mode can reduce possible multi-path interferences [7], polarization mismatch [8] as well as the Faraday rotation effect when propagating through the ionospheric layer [9]. One popular way of generating CP beam radiation is using an array with circularly polarized antenna elements which are fed by either a single or multiple feeding points [10]–[14]. Many sophisticated designs have been presented to improve the CP antenna array performance in terms of the axial ratio (AR), impedance bandwith, antenna gain, sidelobe level, etc. Despite their success, the single-feed CP element generally suffers from relatively narrower AR bandwidth [10]–[12] whereas the multi-feed CP element requires a more complex feeding structure with additional power loss [13], [14].

As is known, an alternative way of generating CP beam radiation is using an array of rotated linearly polarized elements with appropriate excitation phases [15]–[32]. This concept was first presented by Huang in [26] where an array with 2×2 linearly polarized microstrip antennas with element rotations and feeding phases arranged in a $[0, \pi/2, \pi, 3\pi/2]$ fashion is constructed to obtain a relatively wide AR bandwidth. This technique was lately called sequential rotation technique (SRT), and it has been widely extended to the arrays with different elements arranged in circular or even spiral geometries [27]–[30]. In the SRT, the elements are rotated sequentially according to their element positions, and the excitation phases are usually chosen to equal the corresponding rotation angels or the opposite values of rotations for obtaining either left- or right-band CP radiation. It is shown that the planar array configured by using the traditional SRT may have high sidelobe level (SLL) and unacceptable cross-polarization level (XPL) in its diagonal planes (D-plane, i.e, $\phi = 45^\circ$ and 45° pattern cuts for an array aligned in xoy-plane) especially when the beam is steered from the broadside direction. To overcome this problem, a random sequential rotation technique (RSRT) was presented in [31] where all the linearly polarized elements in the array are rotated with random angles within $[0, 2\pi]$, and the best result over different layouts of random rotations is chosen as the final one. The RSRT could effectively avoid the presence of high sidelobe level in the D-plane. In [32], a gradient-based optimization method was introduced to optimize the element rotations for the array including mutual coupling. However, in both [31] and [32], only one CP beam pointing at a fixed direction is considered, which means that the selected distribution of element rotations may be not good enough when the beam direction is changed to

Manuscript received xxx. This work was supported in part by the Natural Science Foundation of China (NSFC) under Grant No. 61871338 and in part by the University of Technology Sydney.

Y. Peng is with the Department of Electronic Science and Institute of Electromagnetics and Acoustics, Xiamen University, Fujian 361005, China.

Y. Liu is with the School of Electronic Science and Engineering, University of Electronic Science and Technology of China, Chengdu 611731, China.

M. Li and Y. Jay Guo are with the Global Big Data Technologies Centre, University of Technology Sydney (UTS), NSW 2007, Australia.

H. Liu is with the School of Electronic and Information Engineering, Xi'an Jiaotong University, Xi'an 710049, China.

another angle. In addition, the excitation phases in [31] and [32] are directly determined according to the rotation angles and the required phase compensation for the given beam direction, and consequently they would not be the optimal. More recently, a constructed analytical phasing (CAP) technique was presented in [33] to efficiently calculate the excitation phases for maximizing the beam gain for a given rotated element distribution and beam pointing direction (the rotation angles are prefixed), but this technique lacks SLL and cross-polarization level control. Besides, some techniques utilize the element rotations to improve SLL or the mainlobe shaping performance but for linearly polarized array patterns [34]–[37]. Besides, related research also includes the application of SRT and RSRT to transmit arrays or metasurface lens for beam focusing or improved XPL in high-gain applications [38]–[40]. However, to the best of our knowledge, no technique for synthesizing CP multi-beam patterns with accurate control of both SLL and XPL by using rotated linearly polarized elements has been reported in the literature.

In this work, we present a novel strategy to obtain the best common element rotations with optimized excitation phases for planar rotated dipole arrays to synthesize multi-beam CP patterns pointing at different directions while controlling both SLL and XPL of each beam pattern. In addition to the common element rotations, the excitation phases for each of CP patterns are also adopted as the optimization variables other than the determined values calculated according to the rotation angles and the required beam pointing direction. This releases many more degrees of synthesis freedom, thus providing the possibility to improve the multiple CP pattern performance. However, this leads to a new problem of demanding excessive computation resources as now there are too many optimization variables for planar arrays with multiple CP beams. To tackle this issue, a two-step rotation and phase optimization strategy is presented. In the first step, the required excitation phase for each CP pattern is approximated as a common phase part plus a prefixed beam focusing phase term, and thus the best common element rotations and common phase parts can be found by solving a multi-beam CP pattern optimization problem which minimizes the difference between the synthesized and desired SLLs, XPLs, as well as the beam pointing deviation. Second, a refining step is performed which re-optimize the additional phase parts individually for each CP beam pattern for the given common element rotations obtained at the first step. In this way, the number of optimization variables in each optimization is significantly reduced.

The proposed two-step optimization strategy explores the rotations and multiple sets of excitation phases for multiple CP patterns as the synthesis freedoms meanwhile maintaining an acceptable computational cost. Several examples of synthesizing single and multiple scanned CP beam patterns for planar rotated dipole arrays with different apertures are provided to validate the effectiveness and advantages of the proposed method. Synthesis results show that the proposed two-step rotation and phase optimization strategy can achieve satisfactory multi-beam CP patterns with much better overall SLL and XPL performance than those achieved by the SRT and RSRT.

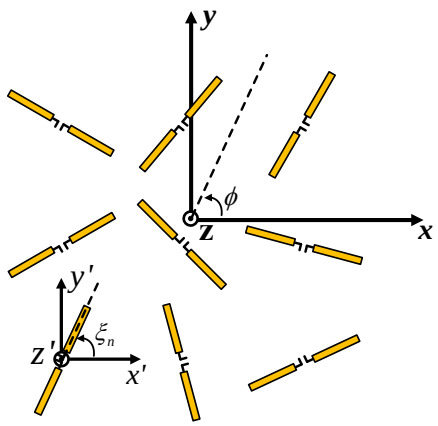

Fig. 1: Configuration of a 3×3 planar array with rotated dipole antennas.

II. Formulation and Algorithm

A. Planar Rotated Dipole Array with Multi-beam CP patterns

Consider a planar array with N rotated dipole antennas located at $\boldsymbol{r}_n = [x_n, y_n]$ for $n = 1, 2, \cdots, N$. As an illustration, Fig. 1 shows a 3×3 element-rotated planar patch array. Suppose the rotation angle for the n element is denoted as $\xi_n \in [0, 2\pi]$ that is measured in counterclockwise way from the x'-axis of the local coordinate system (it is parallel with the x-axis of the global coordinate system as shown in Fig. 1). Assuming that the mutual coupling is ignored, we can write the vectorial pattern for the nth dipole element in the following [35]:

$$E_{n,\theta}(\theta, \phi; \xi_n) = \frac{\cos\theta \cos(\phi - \xi_n) \cos\left(\frac{\pi}{2} \sin\theta \cos(\phi - \xi_n)\right)}{1 - \sin^2\theta \cos^2(\phi - \xi_n)} \tag{1}$$

$$E_{n,\phi}(\theta, \phi; \xi_n) = \frac{-\sin(\phi - \xi_n) \cos\left(\frac{\pi}{2} \sin\theta \cos(\phi - \xi_n)\right)}{1 - \sin^2\theta \cos^2(\phi - \xi_n)} \tag{2}$$

where ϕ is measured from the x-axis in azimuth plane and θ is measured from the z-axis.

Assume that the rotated dipole array generates M beam patterns scanned at different directions, and those patterns share the same element rotations but with different sets of excitation phases. The $\hat{\theta}$- and $\hat{\phi}$- polarized components of the mth scanned pattern can be written as:

$$F_{\theta}^{(m)}(\theta, \phi) = \sum_{n=1}^{N} E_{n,\theta}(\theta, \phi; \xi_n)\, e^{j(\beta \boldsymbol{r}_n \boldsymbol{u}^T(\theta,\phi) + \varphi_n^{(m)})} \tag{3}$$

$$F_{\phi}^{(m)}(\theta, \phi) = \sum_{n=1}^{N} E_{n,\varphi}(\theta, \phi; \xi_n)\, e^{j(\beta \boldsymbol{r}_n \boldsymbol{u}^T(\theta,\phi) + \varphi_n^{(m)})} \tag{4}$$

where $j = \sqrt{-1}$, $\boldsymbol{u}(\theta, \phi) = [\sin\theta\cos\phi, \sin\theta\sin\phi]$, $\beta = 2\pi/\lambda$ is the wavenumber in free space, and $\varphi_n^{(m)}$ is the excitation phase of the nth element for the m pattern. As is known, for an arbitrary radiated field in far-field region, the left-hand (LH) and right-hand (RH) circularly polarized components can be constructed from its $\hat{\theta}$- and $\hat{\phi}$- polarized components. Thus, the LHCP and RHCP components of the

mth array pattern can be obtained as:

$$F_{LH}^{(m)}(\theta,\phi)=\frac{F_{\theta}^{(m)}(\theta,\phi)-jF_{\phi}^{(m)}(\theta,\phi)}{2} \tag{5}$$

$$F_{RH}^{(m)}(\theta,\phi)=\frac{F_{\theta}^{(m)}(\theta,\phi)+jF_{\phi}^{(m)}(\theta,\phi)}{2} \tag{6}$$

By choosing appropriate rotations ξ_n and excitation phases $\varphi_n^{(m)}$, it is possible to make the antenna array radiate multiple LHCP (or RHCP) beam patterns while decreasing the RHCP (or LHCP) components as much as possible.

B. Multi-beam CP Pattern Synthesis Problem Description

The key problem is how to find the best common rotations and multiple sets of phase distributions for radiating multiple CP beam patterns with desired characteristics while suppressing the cross-polarization components. For the SRT, a typical way is dividing the whole antenna array into multiple 2×2 subarrays and then set the rotation angles for each subarray as $[0,-\pi/2,-\pi,-3\pi/2]$ for the RHCP pattern or $[0,\pi/2,\pi,3\pi/2]$ for the LHCP pattern. Meanwhile, the excitation phase is set as:

$$\varphi_n=\xi_n-\beta\boldsymbol{r}_n\boldsymbol{u}^T(\theta_{\max},\phi_{\max}) \tag{7}$$

where $\beta\boldsymbol{r}_n\boldsymbol{u}^T(\theta_{\max},\phi_{\max})$ is the beam focusing phase term for generating a main beam directing to $(\theta_{\max},\phi_{\max})$. However, it has been mentioned that such a configuration results in a possible high SLL and XPL at the D-plane of the obtained pattern [26] due to a relatively large spacing between the subarray in D-plane. Thus, the RSRT presented in [31] introduces random rotations to all the elements in the array, and consequently removes the presence of high SLL and XPL. However, both the SRT and RSRT consider only synthesizing a single CP beam pattern pointing at a fixed direction. In addition, both of them adopt fixed excitation phases that are calculated by the rotation angles plus the beam focusing phase term and, thus, without any optimization. When extended to synthesize multiple CP patterns pointing at different directions, they may have unsatisfactory performance due to limited degrees of synthesis freedoms.

In this work, we choose to optimize both the rotation angles and multiple sets of excitation phases for improving the multi-beam CP pattern performance. Suppose the desired beam direction of the mth CP beam pattern is $(\theta_{\max}^{(m)},\phi_{\max}^{(m)})$, the excitation phase can be construct as

$$\varphi_n^{(m)}=\eta_n^{(m)}-\beta\boldsymbol{r}_n\boldsymbol{u}^T(\theta_{\max}^{(m)},\phi_{\max}^{(m)}) \tag{8}$$

where $\eta_n^{(m)}$ is independent optimization variable, and it is not necessarily equal to ξ_n here. Thus, we choose both ξ_n and $\eta_n^{(m)}$ for $n=1,2,\cdots,N$ and $m=1,2,\cdots,M$ as optimization variables for the multi-beam CP pattern synthesis problem.

To synthesize the desired multi-beam patterns, a objective function that penalizes the SLL, XPL, and the peak direction is constructed here. Assume the desired SLL and XPL for each of M CP patterns are denoted as Γ_{SL} and Γ_X, respectively. The objective function for this problem can be given as follows:

$$\begin{aligned}f=&\frac{W_1}{MB}\sum_{m=1}^{M}\sum_{b^{(m)}=1}^{B^{(m)}}\frac{1}{2}\left(X_{b^{(m)}}^{(m)}+\left|X_{b^{(m)}}^{(m)}\right|\right)^2\\&+\frac{W_2}{MG}\sum_{m=1}^{M}\sum_{g=1}^{G}\frac{1}{2}\left(Y_g^{(m)}+\left|Y_g^{(m)}\right|\right)^2+\frac{W_3}{M}\sum_{m=1}^{M}\left(Z^{(m)}\right)^2\end{aligned} \tag{9}$$

where

$$X_{b^{(m)}}^{(m)}=\left|F_{CO}^{(m)}\left(\theta_{b^{(m)}}^{(m)},\phi_{b^{(m)}}^{(m)}\right)\right|^2-\Gamma_{SL} \tag{10}$$

$$Y_g^{(m)}=\left|F_{X}^{(m)}\left(\theta_g^{(m)},\phi_g^{(m)}\right)\right|^2-\Gamma_X \tag{11}$$

$$\begin{aligned}Z^{(m)}=&-\left|F_{CO}^{(m)}\left(\theta_{\max}^{(m)},\phi_{\max}^{(m)}\right)\right|^2+\\&\frac{\left|\left|F_{CO}^{(m)}\left(\theta_{\max}^{(m)}+\Delta\theta,\phi_{\max}^{(m)}\right)\right|^2-\left|F_{CO}^{(m)}\left(\theta_{\max}^{(m)}-\Delta\theta,\phi_{\max}^{(m)}\right)\right|^2\right|}{\Delta\theta}\end{aligned} \tag{12}$$

In the above, $F_{CO}^{(m)}$ denotes the desired co-polarization (COP) of the mth beam pattern which can be either LHCP or RHCP, depending on the application, and $F_X^{(m)}$ denotes the cross-polarization (XP) component of the mth pattern. $(\theta_{b^{(m)}}^{(m)},\phi_{b^{(m)}}^{(m)})$ for $b^{(m)}=1,2,\cdots,B^{(m)}$ are sampling angles in the sidelobe region of the mth CoP pattern, $(\theta_g^{(m)},\phi_g^{(m)})$ for $g=1,\ 2,\ \cdots$, G are sampling angles in the region of XP pattern for the mth beam. W_1, W_2 and W_3 are the weighting coefficients that are used to penalize the differences between the synthesized and desired results in terms of the SLL, XPL and beam pointing direction, respectively.

Clearly, minimizing the objective function in (9) is a highly nonlinear optimization problem. Some stochastic optimization algorithms with good global searching ability would be appropriate. Here we choose the particle swarm optimization (PSO) since it is a simple but computationally inexpensive and effective algorithm. It has been successfully applied to solve many inverse problems including antenna array synthesis problems [41], [42]. However, it should be noted that the proposed multi-beam CP pattern synthesis problem is very computationally expensive since it involves a large number of unknowns to be optimized. For a N-element planar rotated dipole array with M CP beam patterns, we need to optimize N rotations and $N\times M$ excitation phases. For example, for the case of an 8×8-element array and 15 beam patterns, we have a total of 1024 variables to be optimized. For a highly nonlinear problem with such a huge number of unknowns, it is very hard to be solved if without super-computer source. Hence, we will present a two-step rotation and phase optimization strategy which still releases the excitation phases as the additional degrees of synthesis freedom but keep the problem to be solvable. The detailed description about this strategy will be given in the following.

C. The Proposed Two-Step Element Rotation and Phase Optimization Strategy

As mentioned above, minimizing the objective function (9) by directly optimizing all the ξ_ns and $\eta_n^{(m)}$s is too computationally expensive. Instead, we adopt a two-step rotation and

excitation phase optimization strategy to solve the concerned problem. This strategy consists of the initial optimization step and the refining optimization step which are described as follows.

1) The initial optimization step: For the initial optimization, we assume that the excitation phase of each element for different patterns is approximated as a common phase part plus the beam focusing phase part. That is, the excitation phase is approximated as

$$\varphi_n^{(m)} \approx \eta_n^{\text{approx}} - \beta \boldsymbol{r}_n \boldsymbol{u}^T(\theta_{\max}^{(m)}, \phi_{\max}^{(m)}) \tag{13}$$

Note that although the η_n^{approx} is the same for different patterns, it is not equal to the rotation angle ξ_n. Instead, we use both ξ_n and η_n^{approx} as optimization variables when minimizing the cost function given in (9). Thus, the number of optimization variables in this initial step is $2N$ which is much smaller than the one by directly optimizing all the ξ_ns and $\eta_n^{(m)}$s. However, it should be noted that the proposed initial optimization can obtain much better accuracy performance than the one by simply setting $\varphi_n = \xi_n - \beta \boldsymbol{r}_n \boldsymbol{u}^T(\theta_{\max}^{(m)}, \phi_{\max}^{(m)})$ like in the SRT and RSRT to deal with the multi-beam CP pattern synthesis problem.

2) The refining optimization step: Once the optimal rotations along with the approximated excitation phases are obtained in the initial step, we can refine the excitation phases for each CP beam pattern for the optimized element rotation distribution. In this situation, the excitation phases can be written as:

$$\varphi_n^{(m)} = \delta_n^{(m)} + \eta_n^{\text{approx}} - \beta \boldsymbol{r}_n \boldsymbol{u}^T(\theta_{\max}^{(m)}, \phi_{\max}^{(m)}) \tag{14}$$

where $\delta_n^{(m)}$ is the additional refining phase term for improving each CP beam performance. In this step, we perform the minimization of the objective function (9) again, but only takes $\delta_n^{(m)}$ for $n = 1, \cdots, N$ as the optimization variables for each of beam pattern. That is, in this step, the M beams with different beam directions are synthesized individually. Thus, a total number of M times of optimizations (each with N optimization variables) are performed to refine the $M \times N$ excitation phases which can effectively improve the performance of M beam patterns.

The proposed two-step rotation and phase optimization strategy transforms the original optimization problem with a huge number of unknowns as solving multiple sub-problems, each has much smaller number of unknowns. Nevertheless, the two-step optimization strategy still releases the excitation phases along with the rotations as the synthesis freedoms to improve the multi-beam CP pattern performance.

D. The Proposed Synthesis Procedure

The whole procedure based on the proposed two-step rotation and phase optimization strategy for synthesizing multi-beam CP patterns for a planar rotated dipole array is summarized in Algorithm I. In this procedure, the common element rotation angles $\xi_n \in [0, 2\pi]$ as well as the approximated common phases $\eta_n^{\text{approx}} \in [0, 2\pi]$ for $n = 1, \cdots, N$ are found in Step 4, while those excitation phases are further refined in Step 5 and 6 for each beam pattern. The PSO is chosen to accomplish all the optimizations in this procedure for its simplicity and effectiveness, although some other stochastic algorithms may be also applicable.

Algorithm 1 The Proposed Two-Step Element Rotation and Phase Optimization for Synthesizing Planar Rotated Dipole Array with CP Multi-beam Patterns

1: Initialize the array configuration, including the element count N, beam numbers M, and beam direction $(\theta_{\max}^{(m)}, \phi_{\max}^{(m)})$ for $m = 1, \cdots, M$, and set the desired maximum SLL Γ_{SL} and XPL Γ_X;
2: Set the sidelobe region for the mth beam as $\{(U, V); |(U - U_{\max}^{(m)})^2 + (V - V_{\max}^{(m)})^2 \geq (R_{SL}^{(m)})^2\}$, where $U = \sin\theta\cos\phi$, $V = \sin\theta\sin\phi$, $U_{\max}^{(m)} = \sin\theta_{\max}^{(m)}\cos\phi_{\max}^{(m)}$ and $V_{\max}^{(m)} = \sin\theta_{\max}^{(m)}\sin\phi_{\max}^{(m)}$ is peak direction of the mth beam, $R_{SL}^{(m)}$ is the radius of the mainlobe region of the mth beam in UV plane.
3: Set the parameters for the PSO algorithm such as the maximum iteration M_{iter}, population size N_p, problem dimension D, as well as weighting factors W_1, W_2 and W_3;
4: In the initial optimization step, for the M beams, find the optimal common element rotation angle $\xi_n \in [0, 2\pi]$ and the approximated common phase $\eta_n^{\text{approx}} \in [0, 2\pi]$ for $n = 1, \cdots, N$ by minimizing the cost function (9) using the PSO algorithm;
5: With the rotation angles obtained in the initial step, M times of refining optimization are performed. For each optimization, the mth beam is synthesized by optimizing the refining phase term $\delta_n^{(m)} \in [0, 2\pi]$ for $n = 1, \cdots, N$ by minimizing the cost function (9) using the PSO algorithm;
6: Calculate the optimal phase $\varphi_n^{(m)}$ for each beam by using (14);
7: The optimal multi-beam patterns with desired SLLs and XPLs can be obtained with the common rotation angles optimized in step 4 and excitation phases calculated in step 6.

III. Numerical Results

In this section, to verify the performance and effectiveness of the proposed strategy, four numerical examples of synthesizing CP multi-beam scanning planar arrays with reduced SLLs and suppressed XPLs are presented. The first two examples are synthesizing a steered beam pattern and a two dimensional (2D) multi-beam scanning patterns, respectively, both for the 8×8 dipole array. The third example is synthesizing one dimensional (1D) multi-beam scanning patterns for arrays with different sizes. The last example is synthesizing multi-beam scanning patterns for an array with rotated printed dipole antennas considering practical feeding and metal ground. The obtained rotated printed dipole array is fabricated and measured. Note that, in all of the examples, the maximum number of generations is set as $M_{iter} = 3000$ for the PSO, and the LHCP is considered as the COP whereas the RHCP is considered as the XP. However, the proposed method is also applicable if the RHCP is considered as the COP. Besides, all the synthesis examples are executed on the same work station with Inter(R) Xeon(R) CPU E5-2697 v4 @2.30 GHz.

A. Synthesizing a 8×8 Rotated Dipole Array with a Steered CP Pattern

In the first example, we consider synthesizing a planar rotated dipole array with a single scanned CP pattern that is a special case of multi-beam CP patterns (i.e., $M = 1$). Suppose the array is comprised of 8×8 half-wave dipoles with a uniform spacing of 0.5λ in both $\hat{x}$ and $\hat{y}$ directions.

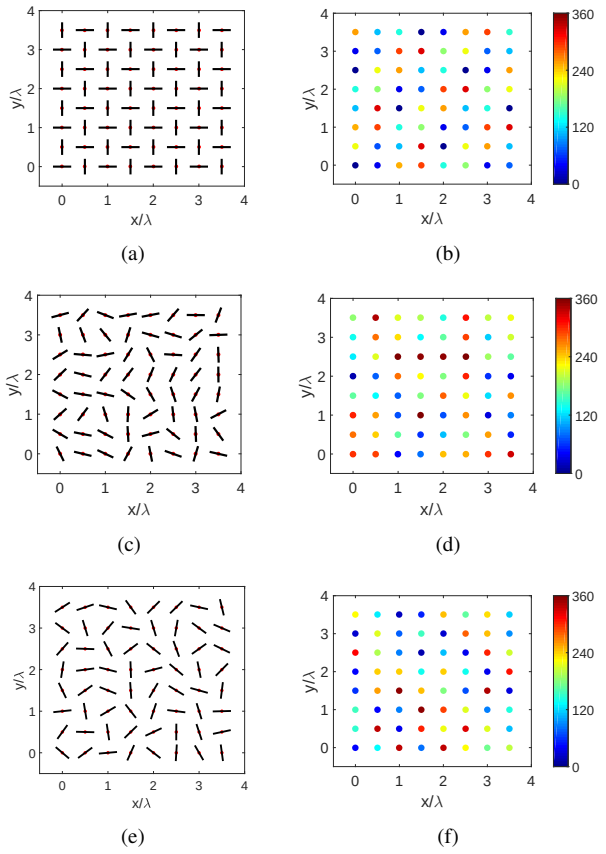

Fig. 2: The rotation angles and excitation phases for the 8×8 planar dipole array. (a) rotation angles and (b) phase distribution obtained by SRT, (c) rotation angles and (d) phase distribution obtained by RSRT, (e) rotation angles and (f) phase distribution obtained by the proposed method.

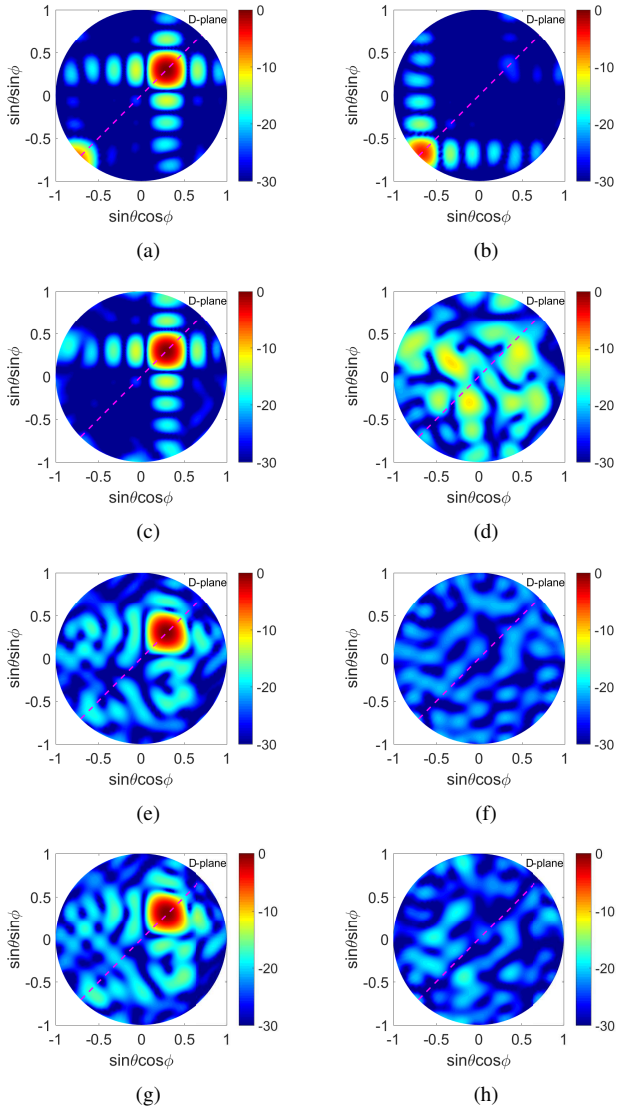

Fig. 3: Top views of the COP and XP patterns obtained by the SRT, the RSRT, and the proposed method in Example A. (a) and (b) show the COP and XP patterns by the SRT, (c) and (d) show the COP and XP patterns by the RSRT, (e) and (f) show the synthesized COP and XP patterns with the proposed method, (g) and (h) show the full-wave simulated COP and XP patterns for the obtained array by the proposed method.

The desired pattern has a LHCP beam that is pointing at the direction of ($\theta_{max} = 25°$, $\phi_{max} = 45°$) in the D-plane. If the conventional SRT is applied to synthesize this scanned CP beam pattern, one typical choice for the rotated dipole geometry is shown in Fig. 2(a) where 16 subarrays are used, each with 2×2 dipoles sequentially rotated with an interval of $\pi/2$. The excitation phase is set as the corresponding dipole's rotation angle plus the beam focusing phase given in (7), as plotted in Fig 2(b). The corresponding COP (LHCP) and XP (RHCP) patterns are shown in Fig. 3(a) and (b), respectively. As can be seen, the COP pattern has a high sidelobe that is actually a grating lobe attributed to the large spacing of subarrays, and the XP pattern also has a high level in the D-plane as expected. The maximum SLL and XPL are -6.47 dB and -4.38 dB, respectively. The RSRT presented in [31] can reduce the high SLL and XPL in the D-plane. We run 200 times of implementations for the random element rotations, and the best result of rotation and excitation phase distributions that gives the lowest SLL and XPL are shown in Fig. 2(c) and (d). Note that the excitation phase is not optimized but calculated according to (7) in the RSRT. The corresponding COP and XP patterns are given in Fig. 3(c) and (d), respectively. The obtained best SLL and XPL over 200 times of runs by the RSRT are -12.52 dB and -10.61 dB, respectively.

Now, we apply the proposed method to synthesize the same CP pattern for further reduced SLL and XPL. For the single beam case, only the first optimization step of the proposed method is required for optimizing both element rotations and phases, and the second refining step is unnecessary. We set $\Gamma_{SL} = -17$ dB and $\Gamma_X = -21$ dB for the desired SLL and XPL, respectively, $R_{SL} = 0.32$ for the mainlobe beamwidth control, $W_1 = 2$, $W_2 = 1$ and $W_3 = 1$ for the weighting coefficients, $D = 128$ for the number of variables, and $N_p = 1.5D = 192$ for the population size. In this example, the proposed method takes 4.2 hours to accomplish the synthesis. The obtained rotation and excitation phase distributions are shown in Fig. 2(e) and (f), respectively. The top views of the corresponding COP and XP patterns are shown in Fig. 3(e) and (f), respectively. The obtained SLL and XPL are -16.86 dB and -20.81 dB, respectively. Both of them are very much lower than the ones obtained by the SRT and

TABLE I
THE SLLS AND XPLS OBTAINED BY ACHIEVED ROTATION RESOLUTION AND PHASE QUANTIZATION ACCURACY IN FIRST EXAMPLE

CP pattern performance	Phase quantization accuracy							
	4-bit		5-bit		6-bit		ideal (accurate)	
Rotation resolution	SLL (dB)	XPL (dB)	SLL (dB)	XPL (dB)	SLL (dB)	XPL (dB)	SLL (dB)	XPL (dB)
5°	-15.24	-17.72	-15.99	-18.91	-16.62	-19.66	-16.70	-20.43
ideal (accurate)	-15.36	-17.98	-16.11	-19.06	-16.68	-19.75	-16.86	-20.81

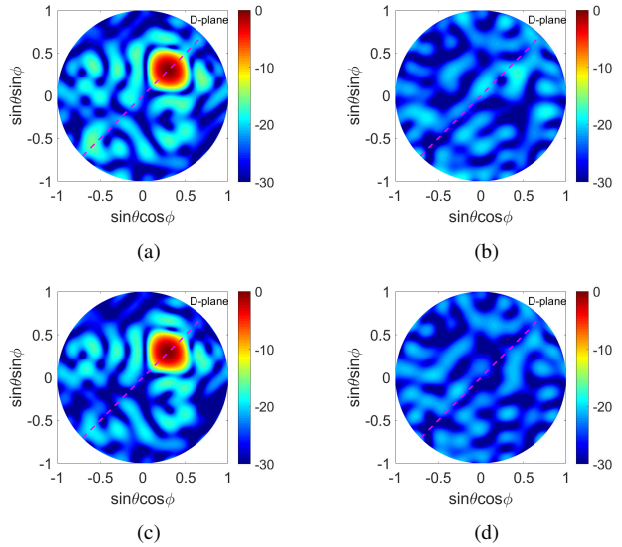

Fig. 4: Top views of the COP and XP patterns obtained by using 4- and 6-bit quantized excitation phases, both with 5° resolution of rotation angles. (a) and (b) show the COP and XP patterns using 4-bit quantized phases, respectively; (c) and (d) show the COP and XP patterns using 6-bit quantized phases, respectively. The corresponding results using accurate phases and rotation angles are given in Fig. 3(e) and (f).

RSRT, which shows the superiority of the proposed method in improving the CP purity and decreasing the SLL of the steered pattern. In addition, the obtained dipole array with the optimized rotation angles and excitation phases is full-wave simulated using the high frequency structure simulator (HFSS) software. The designed dipole model has a length of 48 mm and diameter of 2 mm, working at the frequency of 3 GHz. Fig. 3(g) and (h) show the full-wave simulated COP and XP patterns, respectively. As can be seen, they generally agree well with the synthesized ones except for a little bit degradation in some sidelobe region and XP region due to mutual coupling effect (the simulated maximum SLL and XPL are increased to -14.50 dB and -17.25 dB, respectively).

In addition, we also check the effect of realized accuracies for both rotation angles and excitation phases in practice on the pattern performance. Table I shows the realized SLLs and XPLs for different cases of 4, 5, 6-bit phase quantization at both ideal (accurate) rotation angles and 5° rotation angle resolution. It can be seen that the realized SLL and XPL are indeed affected by both of the phase and rotation angle implementation accuracies. When the achieved resolution of the mechanical rotation is 5°, using 4-bit quantized phases gives 1.62 dB and 3.09 dB degradation in SLL and XPL, respectively, while using 6-bit quantized phases gives only 0.24 dB and 1.15 dB degradation in SLL and XPL, respectively. Fig. 4(a)-(d) show the realized COP and XP patterns for the case of 4 and 6-bit phase quantization and 5° mechanical rotation resolution. As can be seen, the obtained pattern results using 6-bit phase quantization and 5° rotation resolution are approaching very well to the synthesized accurate ones shown in Fig. 3(e) and (f).

B. Synthesizing a 8×8 Rotated Dipole Array with Multi-beam CP Patterns

In the second example, we check the effectiveness of the proposed method for synthesizing multi-beam CP patterns with different peak directions using a planar rotated dipole array. Assume that a total number of $M = 15$ CP patterns are desired, with their beams directing to the angles given in the first column of Table II. In this example, 8×8 rotated dipoles with a spacing of $\lambda/2$ are still used. At first, the SRT and the RSRT are extended to synthesize the multi-beam CP pattern as an comparison. The dipole rotations and excitation phases for the SRT are arranged the same as those in the first example. For the RSRT, we also run 200 times of random distributions, and pick up the best one as the final result. The SLLs and XPLs obtained by the SRT and RSRT for all the 15 CP patterns are given in the left columns of Table II. As can be seen, for the SRT, the broadside beam pattern has the lowest SLL and XPL among the 15 beam patterns. However, the SLL and especially the XPL are increased as the beam is steered from the broadside direction. When the beam is steered to $\theta_{\max} = 30^\circ$, the SLLs and XPLs are respectively increased to -9.11 dB and -8.65 dB for $\phi_{\max} = [0^\circ, 90^\circ, 180^\circ, 270^\circ]$, and they are even increased to -7.89 dB and -2.85 dB respectively, for $\phi_{\max} = [45^\circ, 135^\circ, 225^\circ, 315^\circ]$ in D-plane. On the other hand, the RSRT can significantly remove the extremely high SLL and XPL problem for the beam pattern scanning in the D-plane, but the obtained SLLs for different beam patterns are ranging from -13.07 dB to -12.03 dB, and the XPLs are ranging from -13.5 dB to -11 dB. They are still unsatisfactory for usual applications.

Then we apply the proposed method to synthesize the same CP multi-beam patterns by using the 8×8 rotated dipole array as well. In this case, two step optimizations are utilized. In the first step, the common rotations and approximated excitation phases are optimized by using PSO with $D = 128$, $N_p = 1.5D = 192$. In the second step, the excitation phases are refined for each beam pattern for the obtained rotated array geometry in the first step, and we set $D = 64$, $N_p = 1.5D = 96$ for the PSO. In both steps, we set $R_{SL} = 0.32$ for the mainlobe regions of all 15 beams, $\Gamma_{SL} = -16$ dB and $\Gamma_X = -17$ dB for the desired SLL

TABLE II
THE SLLS AND XPLS OF THE MULTI-BEAM SCANNING PATTERNS OBTAINED BY THE THREE METHODS IN THE SECOND EXAMPLE.

$(\theta_{\max},\phi_{\max})$	SRT		RSRT		The proposed method (initial)		The proposed method (refined)	
	SLL (dB)	XPL (dB)	SLL (dB)	XPL (dB)	SLL (dB)	XPL (dB)	SLL (dB)	XPL (dB)
(0°, 0°)	−13.22	−20.60	−13.07	−13.40	−15.05	−16.54	−15.08	−16.62
(15°, 0°)	−12.63	−17.42	−12.64	−12.37	−14.71	−15.79	−16.00	−17.00
(15°, 60°)	−12.70	−13.24	−12.74	−12.69	−14.71	−15.89	−16.00	−17.00
(15°, 120°)	−12.70	−13.18	−12.67	−12.97	−14.67	−15.68	−16.00	−17.00
(15°, 180°)	−12.62	−17.42	−12.64	−13.32	−14.71	−15.89	−15.60	−16.81
(15°, 240°)	−12.70	−13.24	−12.73	−13.33	−14.81	−15.87	−16.00	−17.00
(15°, 300°)	−12.70	−13.18	−12.68	−12.99	−14.77	−15.89	−15.90	−16.94
(30°, 0°)	−9.11	−8.65	−12.03	−11.44	−14.08	−14.32	−14.41	−16.13
(30°, 45°)	−7.89	−2.85	−12.26	−11.35	−14.52	−13.38	−15.60	−16.68
(30°, 90°)	−9.11	−8.65	−12.00	−12.42	−13.99	−14.78	−15.39	−16.64
(30°, 135°)	−7.89	−2.85	−12.17	−12.20	−14.39	−13.48	−14.51	−15.94
(30°, 180°)	−9.11	−8.65	−12.03	−12.86	−14.09	−14.12	−15.40	−16.61
(30°, 225°)	−7.89	−2.85	−12.27	−12.42	−14.69	−13.65	−14.79	−16.22
(30°, 270°)	−9.11	−8.65	−12.04	−12.17	−14.08	−14.63	−14.63	−15.97
(30°, 315°)	−7.89	−2.85	−12.15	−12.03	−14.55	−13.18	−15.30	−16.34

and XPL, respectively. For optimizing 15 CP beam patterns of the planar rotated array, the proposed method takes 16.8 and 19.7 hours to accomplish the initial and refining steps, respectively. The obtained SLLs and XPLs for the 15 CP beam patterns in the initial and refining steps are given in the right columns of Table II. It can be seen that by using the proposed method, the obtained SLLs for different beams are ranging from -15.05 dB to -13.99 dB in the initial step, and after the refining step, the SLLs are further reduced to be within $[-16.00, -14.41]$ dB which is much lower than the SLL range of $[-13.22, -7.89]$ dB by the SRT as well as $[-13.07, -12.03]$ dB by the RSRT. The XPLs obtained by the proposed method for different beams are ranging within $[-16.54, -13.18]$ dB in the initial step, and after the refining step, they are further reduced to be within $[-17.00, -15.94]$ dB that is much lower than the XPL of $[-13.40, -11.35]$ dB achieved by the RSRT. Compared with the SRT, the proposed method has shown its significant advantage in achieving low SLL and XPL for the beam pointing at $\theta_{\max} = 30^\circ$ and all different $\phi_{\max}$s. As an illustration, Fig. 5(a), (c), (e) and (g) show the summation of the synthesized 15 COP patterns with different beam directions obtained by the SRT, RSRT, the initial and refining steps of the proposed method, respectively. Fig. 5(b), (d), (f), and (h) show the summation of the XP patterns obtained by the SRT, RSRT, the initial and refining steps of the proposed method, respectively. Note that since these results are the summations of all the 15 beam patterns for either COP and XP components, the SLL and XPL values shown in these figures are actually higher than their real values for each pattern. As an example, Fig. 6(a)-(h) show the COP and XP patterns obtained by the three methods for the beam direction at ($\theta_{\max} = 30^\circ$, $\phi_{\max} = 315^\circ$). From Fig. 5 and 6, one can see clearly the better performance of the proposed method over the SRT and RSRT. Similarly, Fig. 6(g) and (h) show the full-wave simulated COP and XP patterns, respectively. As can be seen, they generally agree well with the synthesized ones except for a little bit degradation in some sidelobe region and XP region due to mutual coupling effect. The simulated maximum SLL and XPL are increased to -14.60 dB and -14.45 dB, respectively. The synthesized rotation angles and excitation phases for the 8×8 dipole planar array when the main beam is steered to ($\theta_{\max} = 30^\circ$, $\phi_{\max} = 315^\circ$) are shown in Fig. 7(a) and (b).

Besides, we have also checked the obtained AR performance for all the obtained multi-beam CP patterns by the proposed method. It is found that all the obtained CP patterns in the 3-dB mainlobe region meet the requirement of $AR \leq 3$ dB. As an illustration, Fig. 8(a)-(d) show the obtained regions of $AR \leq 3$ dB for four cases of beam pointing at ($\theta_{\max} = 0^\circ$, $\phi_{\max} = 0^\circ$), ($\theta_{\max} = 15^\circ$, $\phi_{\max} = 300^\circ$), ($\theta_{\max} = 30^\circ$, $\phi_{\max} = 135^\circ$), and ($\theta_{\max} = 30^\circ$, $\phi_{\max} = 315^\circ$), respectively. As can be seen, the obtained regions of $AR \leq 3$ dB for the four cases cover very well their 3-dB mainlobe regions, and the ARs at the maximum beam directions are all close to 1 dB, which validates the good CP characteristics of the mainlobe patterns.

C. Synthesizing Multi-Beam CP Pattern Dipole Arrays with Different Sizes

In the third example, we consider synthesizing the 1D multi-beam patterns scanned from -45° to 45° for rotated dipole arrays with three different sizes which have 8×2, 16×2 and 32×2 elements, respectively. For these three arrays, all the elements are arranged in xoy-plane with a spacing of 0.5λ. The number of beams M are set as 7, 13, and 25, respectively. The scanning and observation plane is fixed as the principle xoz plane ($\phi = 0^\circ$ cut-plane). In this example, the SRT, the RSRT and the proposed method are also utilized to synthesize the same multi-beam patterns with the same array configurations for comparison. For the RSRT, we still run 200 times of random rotation angle distributions and choose the best result for each of the three arrays. For the

TABLE III
THE OBTAINED BEST AND WORST SLLS AND XPLS FOR ARRAYS WITH DIFFERENT SIZES OBTAINED BY THE THREE METHODS IN THE THIRD EXAMPLE.

Array size	M	SRT		RSRT		The proposed method (initial)		The proposed method (refined)	
		SLL (dB) max/min	XPL (dB) max/min	SLL (dB) max/min	XPL (dB) max/min	SLL (dB) max/min	XPL (dB) max/min	SLL (dB) max/min	XPL (dB) max/min
8×2	7	$-11.45/-13.22$	$-12.17/-28.22$	$-11.40/-12.62$	$-9.89/-12.47$	$-18.76/-20.79$	$-18.91/-21.88$	$-20.32/-21.15$	$-21.20/-22.74$
16×2	13	$-12.31/-13.11$	$-12.64/-32.89$	$-12.97/-13.73$	$-10.41/-11.58$	$-19.78/-21.24$	$-19.92/-23.05$	$-20.78/-21.43$	$-21.40/-23.15$
32×2	25	$-12.80/-13.55$	$-12.82/-38.02$	$-12.79/-13.58$	$-12.37/-13.53$	$-20.75/-21.55$	$-19.96/-23.05$	$-21.70/-22.93$	$-22.73/-23.95$

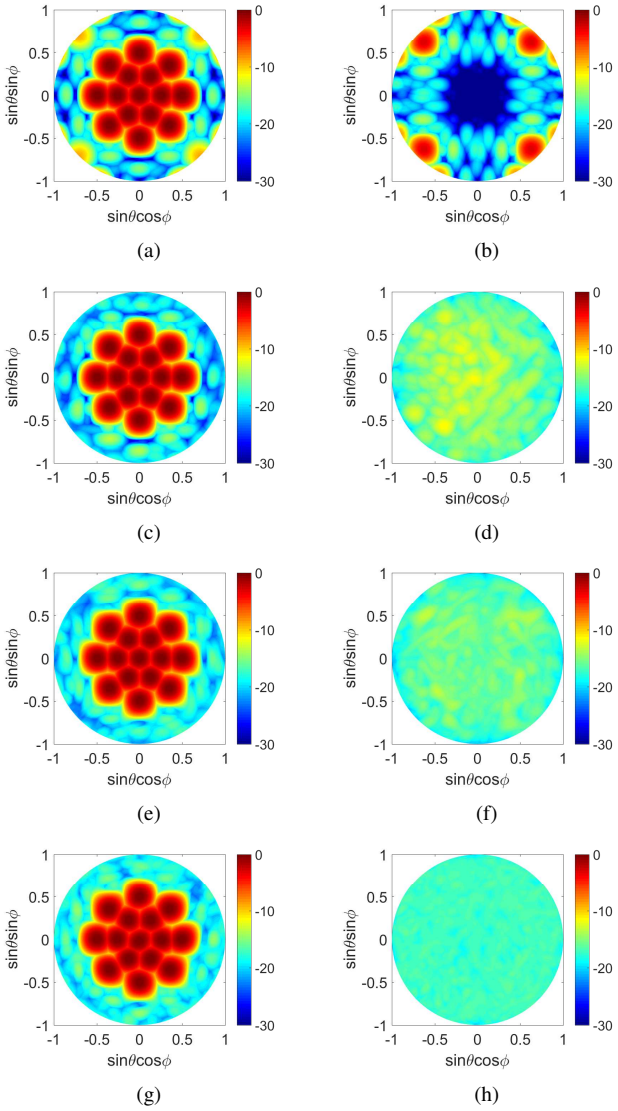

Fig. 5: Top views of the multi-beam scanning COP and XP patterns obtained by the SRT, the RSRT and the proposed method. (a) and (b) show the COP and XP patterns by the SRT; (c) and (d) show the COP and XP patterns by the RSRT; (e)-(h) show the COP and XP patterns by the proposed method in the initial step and refining steps, respectively.

proposed method, the initial and the refined optimization steps are applied for all of the three arrays. In the initial optimization step, for the 8×2, 16×2 and 32×2 rotated dipole arrays, the problem dimensions are set as $D = [32, 64, 128]$, and the population sizes are set as $N_p = [48, 96, 192]$, respectively. In the refining optimization step, the problem dimensions are set as $D = [16, 32, 64]$ and the population sizes are set as $N_p = [24, 48, 96]$ for the three sizes of arrays, respectively.

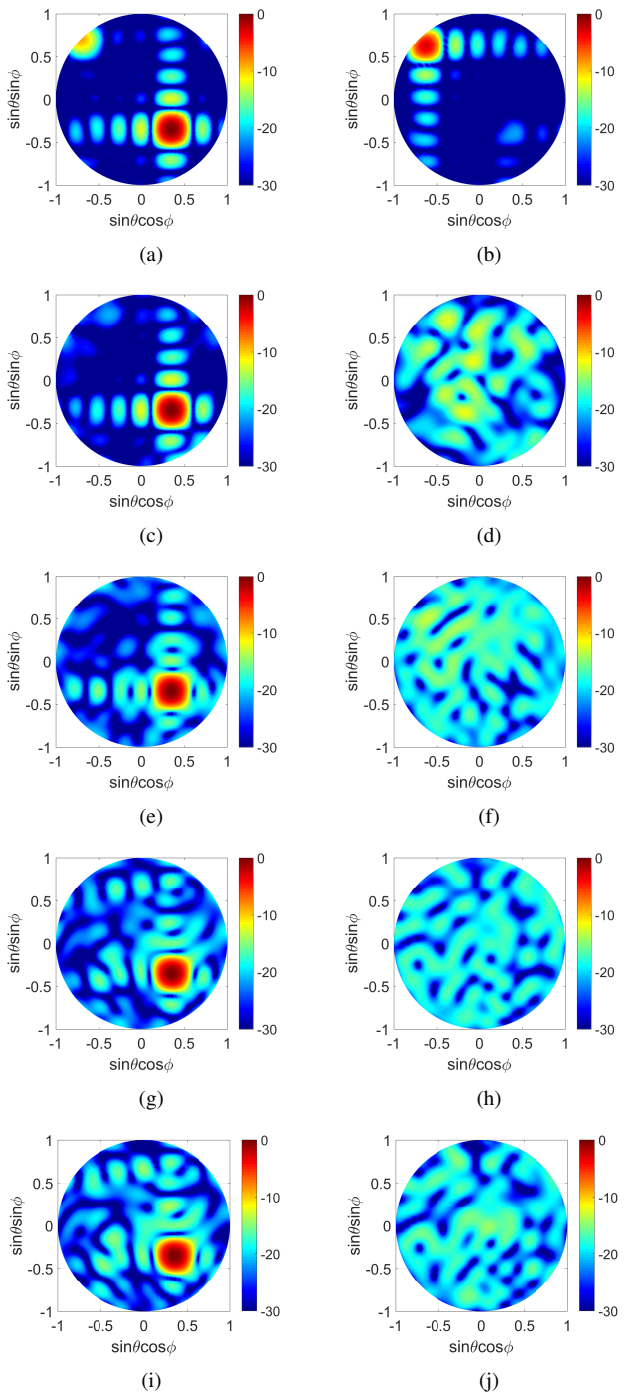

Fig. 6: Top views of the obtained COP and XP patterns when the main beam is steered to ($\theta_{\max} = 30^\circ$, $\phi_{\max} = 315^\circ$) obtained by the SRT, the RSRT and the proposed method. (a) and (b) show the COP and XP patterns by the SRT; (c) and (d) show the COP and XP patterns by the RSRT; (e)-(h) show the COP and XP patterns by the proposed method in the initial step and refining steps, respectively; (i) and (j) show the full-wave simulated COP and XP patterns for the obtained array by the proposed method.

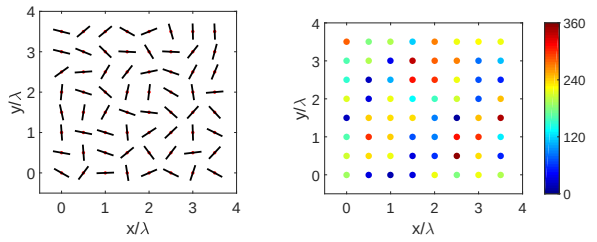

Fig. 7: The synthesized rotation angles and excitation phases for the 8×8 dipole planar array when the main beam is steered to ($\theta_{max} = 30^\circ$, $\phi_{max} = 315^\circ$) in the second example. (a) rotation angles and (b) excitation phase distribution.

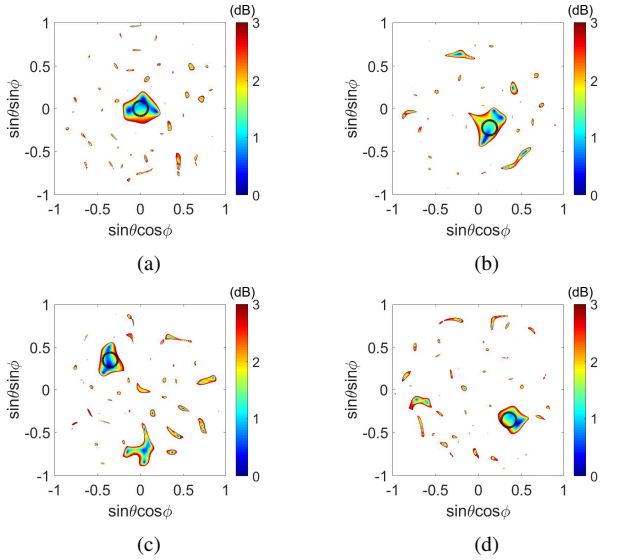

Fig. 8: Top view of the regions for $AR \leq 3$ dB of four different beam patterns in Example B. (a)-(d) show the regions of $AR \leq 3$ dB for the beam pointing at ($\theta_{\max} = 0^\circ$, $\phi_{\max} = 0^\circ$), ($\theta_{\max} = 15^\circ$, $\phi_{\max} = 300^\circ$), ($\theta_{\max} = 30^\circ$, $\phi_{\max} = 135^\circ$) and ($\theta_{\max} = 30^\circ$, $\phi_{\max} = 315^\circ$), respectively. The back circles denote the corresponding 3-dB mainlobe regions.

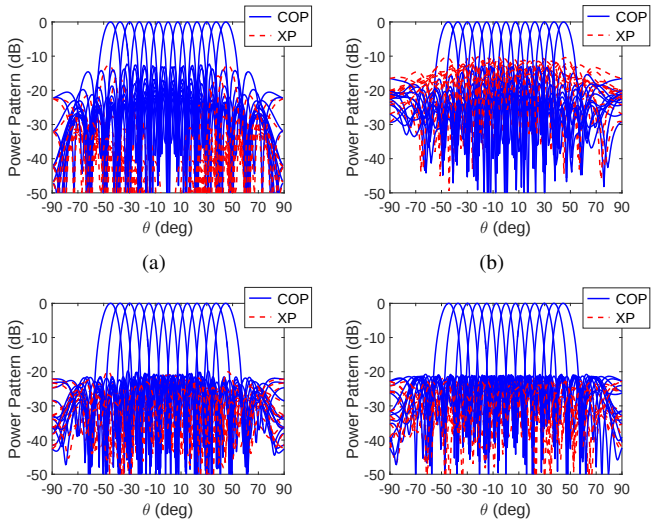

Fig. 9: The COP and XP patterns scanned from -45° to 45° with an interval of 7.5° for an 16×2 planar dipole array obtained by the three methods. (a) patterns obtained by the SRT, (b) patterns obtained by the RSRT, (c) and (d) are patterns obtained by the proposed method in the initial step and refined step, respectively.

In both steps, $\Gamma_{SL} = \Gamma_X = -22$ dB are set for the desired SLL and XPL for all the three sizes of arrays. The weighting factors are set as $W_1 = 1$, $W_2 = 1$ and $W_3 = 1$, respectively.

The SLLs and XPLs obtained by the three methods for the three sizes of arrays are summarized in Table III. It can be seen from the horizontal comparison that, for the $\phi = 0^\circ$ cut of pattern, the RSRT could not obtain lower SLL results than the SRT for all of the three arrays. It indicates that the RSRT is not appropriate for the SLL suppression in the $\phi = 0^\circ$ cut, although it can remove the gratinglobe problem in D-plane as mentioned before. For our proposed method, taking the 16×2 array as an example, the obtained SLLs for different beam patterns are ranging from -21.24 dB to -19.78 dB in the initial step, and after the refining step, the SLLs are further reduced to be within $[-21.43, -20.78]$ dB. The results are much lower than the SLL range of $[-13.11, -12.31]$ dB by the SRT as well as $[-13.73, -12.97]$ dB by the RSRT. On the other hand, the XPLs obtained by the proposed method for different beams are ranging in $[-23.05, -19.92]$ dB in the initial step, and after the refining step, they are further reduced to be within $[-23.15, -21.40]$ dB that is much lower than $[-11.58, -10.41]$ dB achieved by the RSRT. Clearly, the XPL performance by the proposed method is also much better than the range of $[-32.89, -12.64]$ dB by the SRT since its highest XPL among different beams is usually not acceptable. As an illustration, Fig. 9 shows the synthesized multi-beam patterns by the three methods for the array with 16×2 elements. Note that the similar relative performance advantage can be also achieved for the arrays with 8×2 and 32×2 rotated dipoles, as shown in Table III. However, due to limited space, the synthesized multi-beam patterns for these two sizes of arrays have been omitted. In this example, the total time cost for the proposed method including the initial and refining optimization steps is 0.75 hour for the 8×2 array with 7 CP beams, 4.1 hours for the 16×2 array with 13 CP beams, and 18.9 hours for the 32×2 array with 25 CP beams.

D. Synthesizing a CP Multi-beam Rotated Printed Dipole Array Considering Feeding and Metal Ground

In the last example, we check the effectiveness of the proposed method for synthesizing multi-beam CP patterns for rotated printed dipole array considering practical feeding and metal ground. The desired muti-beam CP patterns are assumed to be pointing at $\theta_{\max} = 25^\circ$, 40°, and 50° at the $\phi = 0^\circ$ plane. The triple-beam patterns were obtained in [26] by using 8×2 rectangle microstrip patch antennas arranged by the SRT. The array in [26] works at 2.27 GHz, and the element spacing is 72.71 mm that is about 0.55λ at 2.27 GHz. Here, we adopt a printed dipole antenna loaded with metal ground as the array element, and the antenna structure and its parameters are shown in Fig. 11. The vectorial element pattern for this antenna can be approximated by using the antenna image principle [43]. That is given by:

$$E_{n,\theta}^{\mathrm{GND}}(\theta, \phi; \xi_n) = E_{n,\theta}(\theta, \phi; \xi_n)(1 - e^{-j\beta 2H \cos\theta}) \quad (15)$$

$$E_{n,\phi}^{\mathrm{GND}}(\theta, \phi; \xi_n) = E_{n,\phi}(\theta, \phi; \xi_n)(1 - e^{-j\beta 2H \cos\theta}) \quad (16)$$

TABLE IV
THE SYNTHESIZED, SIMULATED AND MEASURED SLLS AND XPLS BY THE PROPOSED METHOD IN EXAMPLE D AS WELL AS THE RESULTS OBTAINED IN [26].

$(\theta_{\max},\phi_{\max})$	SRT in [26]				The proposed method					
	Calculated*		Measured*		Synthesized		Full-wave simulated		Measured	
	SLL (dB)	XPL (dB)	SLL (dB)	XPL (dB)	SLL (dB)	XPL (dB)	SLL (dB)	XPL (dB)	SLL (dB)	XPL (dB)
$(25^\circ, 0^\circ)$	-11.58	-27.49	-11.70	-25.84	-20.14	-18.74	-17.14	-19.98	-15.69	-17.84
$(40^\circ, 0^\circ)$	-10.90	-18.41	-11.17	-19.90	-18.81	-20.23	-17.00	-19.97	-14.81	-17.25
$(50^\circ, 0^\circ)$	-6.39	-9.07	-7.95	-15.59	-11.18	-18.91	-10.91	-19.74	-12.86	-17.51

*The calculated and measured SLLs and XPLs in [26] are exacted from the corresponding pattern curves presented in this paper.

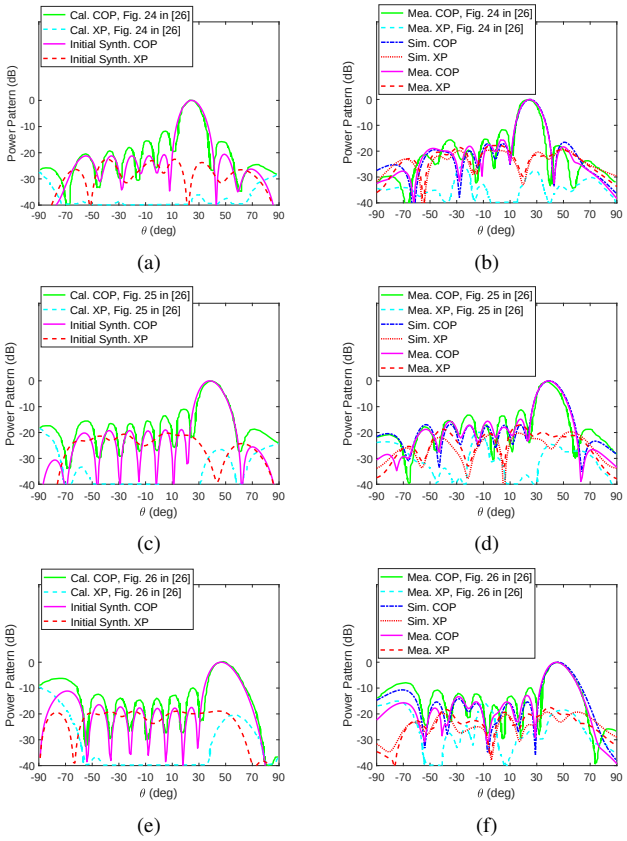

Fig. 10: The initial synthesized, full-wave simulated and measured COP and XP patterns as well as the calculated and measured results in [26]. (a), (c) and (e) show the synthesized results by the proposed method and the calculated results in [26] for the beam pointing at $\theta_{\max} = 25^\circ$, 40° and 50°, respectively; (b), (d) and (f) show the full-wave simulated and measured results by the proposed method and the measured results in [26] for the beam pointing at $\theta_{\max} = 25^\circ$, 40° and 50°, respectively.

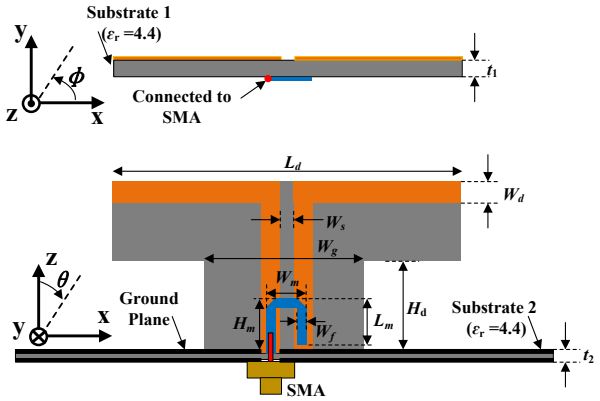

Fig. 11: Geometry of a printed dipole working at 2.27 GHz. The parameters are given as follows: $H_d = 30, H_m = 8, W_d = 5, L_d = 66, L_m = 8.5, W_s = 2, Wg = 10, W_m = 8, W_f = 1.91, t_1 = 1$, and $t_2 = 2$. (Unit:mm)

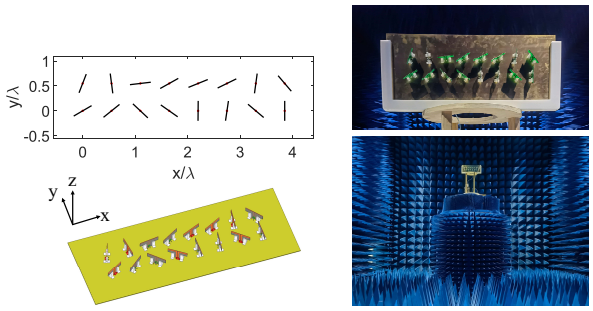

Fig. 12: (a) The obtained rotation angle distribution in example D, (b) The prototype of the 8×2-element rotated printed dipole antenna array in a microwave anechoic chamber.

By replacing the equation (1) and (2) with the above new element pattern expressions, the proposed formulation is still effective for synthesizing the rotated practical dipole antenna array. A total of 8×2 printed dipole elements with the same spacing as that in [26] are used, and their rotations and excitation phases are optimized by using the proposed method. The initial synthesized COP and XP patterns by the proposed method for the three beams ($\theta_{\max} = 25^\circ$, 40°, and 50°) as well as the calculated patterns obtained in [26] are shown in Fig. 10(a), (c), and (e). As can be seen, the synthesized maximum SLLs for all the three beam cases are much lower than the calculated SLLs obtained in [26]. The synthesized XPLs by the proposed method for the three beams are all less than -18 dB, while the calculated XPL of the array in [26] vary significantly with different beams and the XPL for the beam of $\theta_{\max} = 50^\circ$ becomes much higher than other two beam cases. The statistics of the obtained SLL and XPL by the proposed method as well as the results extracted from [26] is given in Table IV for detailed comparison.

The obtained printed dipole array with optimized rotation angles is built and full-wave simulated in HFSS, and the array model with the rotation angle distribution is shown in Fig. 12(a). Then, we fabricate the 16 printed dipole antennas and mount them with the required rotations on a 2 mm thick double-sided copper clad laminate (play as a metal ground) with size of 708.97 mm $\times$ 272.71 mm. Each element is fed by using SMA connector underneath the ground. The excitation phases are obtained by the proposed refining optimization but

using 16 full-wave simulated active element patterns, which can compensate the pattern performance degradation to some extent. This antenna array prototype is measured using a far-field measurement system in a microwave anechoic chamber located at Haiyun Campus, Xiamen University, as shown in Fig. 12(b). The simulated and measured array patterns are obtained by using simulated and measured active element patterns with the obtained excitation phases. Fig. 10(b), (d) and (f) show the full-wave simulated and measured COP and XP patterns as well as the measured results in [26] for the three different beam cases, respectively. The maximum SLLs and XPLs of these pattern results are also summarized in Table IV. As can be seen, although the measured COP patterns have a little bit higher SLLs than the simulated patterns, they are generally in a good agreement, which validates the effectiveness of the proposed method for practical rotated dipole array design. Compared with the results in [26], the proposed design has a little bit degradation in measured XPLs, but with much better performance in the measured SLLs for all the three beam patterns.

IV. Conclusion

In this paper, a novel method of synthesizing CP multi-beam patterns with reduced SLL and XPL by optimizing the element rotations and excitation phases for planar dipole arrays has been presented. Different from the SRT and RSRT where the excitation phases are calculated according to the rotation angles, multiple sets of phases are adopted as optimization variables to release many more degrees of freedoms for improved performance of the obtained CP multi-beam patterns. In addition, a two-step optimization strategy has been presented to effectively solve the CP multi-beam synthesis problem involved with optimization of a large number of element rotations and excitation phases. Four synthesis examples have been conducted to demonstrate the effectiveness and advantages of the proposed method for synthesizing different CP multi-beam patterns. The results show that the proposed method can effectively overcome the problem of high SLL and XPL that is usually arising in the D-plane of the pattern synthesized by the conventional SRT. And also, the proposed method can obtain much lower SLLs and XPLs than the RSRT due to the optimization of both the common element rotations and all of the excitation phases for multiple CP beam patterns. One prototype of a rotated printed dipole array has been fabricated, and the measured multi-beam CP patterns are in good agreement with the simulated results.

References

[1] A. García-Aguilar, J.-M. Inclán-Alonso, L. Vigil-Herrero, J.-M. Fernández-González, and M. Sierra-Pérez, "Low-profile dual circularly polarized antenna array for satellite communications in the X band," *IEEE Trans. Antennas Propag.*, vol. 60, no. 5, pp. 2276-2284, May 2012.

[2] P. Naseri, S. A. Matos, J. R. Costa, and C. A. Fernandes, "Phase delay versus phase-rotation cells for circular polarization transmit arrays application to satellite Ka-band beam steering," *IEEE Trans. Antennas Propag.*, vol. 66, no. 3, pp. 1236-1247, Mar. 2018.

[3] Y. Zhou, C.-C. Chen, and J. L. Volakis, "Single-fed circularly polarized antenna element with reduced coupling for GPS arrays," *IEEE Trans. Antennas Propag.*, vol. 56, no. 5, pp. 1469-1472, May. 2008.

[4] J. Hur, G. Byun, and H. Choo, "Design of parabola-shaped planar lossy magnetic surface for improved isolation characteristic between GPS array elements with circular polarization property," *IEEE Antennas Wireless Propag. Lett.*, vol. 19, no. 1, pp. 139-142, Jan. 2020.

[5] J.-H. Lee *et al.*, "Noninvasive biosignal detection radar system using circular polarization," *IEEE Trans. Inf. Technol. Biomed*, vol. 13, no. 3, pp. 400-404, May 2009.

[6] V. Wissan *et al.*, "Development of circularly polarized array antenna for synthetic aperture radar sensor installed on UAV," *Prog. Electromagn. Res. C*, vol. 19, pp. 119-133, Jan. 2011.

[7] T. Manabe, K. Sato, H. Masuzawa, K. Taira, T. Ihara, Y. Kasashima, and K. Yamaki, "Polarization dependence of multipath propagation and high-speed transmission characteristics of indoor millimeter-wave channel at 60 GHz," *IEEE Trans. Veh. Technol.*, vol. 44, no. 2, pp. 268-274, May. 1995.

[8] H. Sun and W. Geyi, "A new rectenna with all-polarization-receiving capability for wireless power transmission," *IEEE Antennas Wireless Propag. Lett.*, vol. 15, pp. 814-817, Sep. 2015.

[9] J. L. Volakis, *Antenna Engineering Handbook.* New York, NY, USA: McGraw-Hill, 2007.

[10] P. Sharma and K. Gupta, "Analysis and optimized design of single feed circularly polarized microstrip antennas," *IEEE Trans. Antennas Propag.*, vol. 31, no. 6, pp. 949-955, Nov. 1983.

[11] H. Iwasaki, "A circularly polarized small-size microstrip antenna with a cross slot," *IEEE Trans. Antennas Propag.*, vol. 44, no. 10, pp. 1399-1401, Oct. 1996.

[12] J.-H. Lu, C.-L. Tang, and K.-L. Wong, "Single-feed slotted equilateral-triangular microstrip antenna for circular polarization," *IEEE Trans. Antennas Propag.*, vol. 47, no. 7, pp. 1174-1178, Jul. 1999.

[13] T. Chiba, Y. Suzuki, and N. Miyano, "Suppression of higher modes and cross polarized component for microstrip antennas," *IEEE Antennas Propagat. Soc. Int. Symp. Dig.*, vol. 20, pp. 285-288, May. 1982.

[14] A. Narbudowicz, X. Bao, and M. J. Ammann, "Dual circularly-polarized patch antenna using even and odd feed-line modes," *IEEE Trans. Antennas Propag.*, vol. 61, no. 9, pp. 4828-4831, Sep. 2013.

[15] Fuchs, Benjamin, and J. Jacques, "Optimal polarization synthesis of arbitrary arrays with focused power pattern." *IEEE Trans. Antennas Propag.*, vol. 59, no. 12, pp. 4512-4519, Dec. 2011.

[16] G. Bogdan, P. Bajurko, and Y. Yashchyshyn, "Time-modulated antenna array with dual-circular polarization," *IEEE Antennas Wireless Propag. Lett.*, vol. 19, no. 11, pp. 1872-1875, Jun. 2020.

[17] Kraft and U.R, "Main-beam polarization properties of four-element sequential-rotation arrays with arbitrary radiators," *IEEE Trans. Antennas Propag.*, vol. 44, no. 4, pp. 515-522, Apr. 1996.

[18] A. Zamanifekri and A. B. Smolders, "Beam squint compensation in circularly polarized offset reflector antennas using a sequentially rotated focal-plane array," *IEEE Antennas Wireless Propag. Lett.*, vol. 14, pp. 815-818, Mar. 2015.

[19] D.-F. Guan, C. Ding, Z.-P. Qian, Y.-S. Zhang, Y. J. Guo, and K. Gong, "Broadband high-gain siw cavity-backed circular-polarized array antenna," *IEEE Trans. Antennas Propag.*, vol. 64, no. 4, pp. 1493-1497, Apr. 2016.

[20] S. X. Ta and I. Park, "Compact wideband sequential-phase feed for sequentially rotated antenna arrays," *IEEE Antennas Wireless Propag. Lett.*, vol. 16, pp. 661-664, Aug. 2016.

[21] A. B. Smolders, R. M. C. Mestrom, A. C. F. Reniers, and M. Geurts, "A shared aperture dual-frequency circularly polarized microstrip array antenna," *IEEE Antennas Wireless Propag. Lett.*, vol. 12, pp. 120-123, Jan. 2013.

[22] A. K. Bhattacharyya, "Comparison between arrays of rotating linearly polarized elements and circularly polarized elements," *IEEE Trans. Antennas Propag.*, vol. 56, no. 9, pp. 2949-2954, Sep. 2008.

[23] A. B. Smolders and U. Johannsen, "Axial ratio enhancement for circularly-polarized millimeter-wave phased-arrays using a sequential rotation technique," *IEEE Trans. Antennas Propag.*, vol. 59, no. 9, pp. 3465-3469, Sep. 2011.

[24] B. Zhang, Y. P. Zhang, D. Titz, F. Ferrero, and C. Luxey, "A circularly-polarized array antenna using linearly-polarized sub grid arrays for highly-integrated 60-GHz radio," *IEEE Trans. Antennas Propag.*, vol. 61, no. 1, pp. 436-439, Jan. 2013.

[25] R. F. Ma, Z. H. Jiang, Y. Zhang, X. Y. Wu, T. Yue, W. Hong, and D. H. Werner, "Theory, design, and verification of dual-circularly-polarized dual-beam arrays with independent control of polarization: A generalization of sequential rotation arrays," *IEEE Trans. Antennas Propag.*, vol. 69, no. 3, pp. 1369-1382, Mar. 2021.

[26] J. Huang, "A technique for an array to generate circular polarization with linearly polarized elements," *IEEE Trans. Antennas Propag.*, vol. 34, no. 9, pp. 1113-1124, Sep. 1986.
[27] H. Iwasaki, T. Nakajima, and Y. Suzuki, "Gain improvement of circularly polarized array antenna using linearly polarized elements," *IEEE Trans. Antennas Propag.*, vol. 43, no. 6, pp. 604-608, Jun. 1995.
[28] P. Hall and M. Smith, "Sequentially rotated arrays with reduced sidelobe levels," *IEE Proc. Microw. Antennas Propag*, vol. 141, no. 4, pp. 321-325, Aug. 1994.
[29] H. K. Kan and R. B. Waterhouse, "A small CP-printed antenna using 120° sequential rotation," *IEEE Trans. Antennas Propag.*, vol. 50, no. 3, pp. 398-399, Aug. 2002.
[30] S. Liao and Q. Xue, "Compact UHF three-element sequential rotation array antenna for satcom applications," *IEEE Trans. Antennas Propag.*, vol. 65, no. 5, pp. 2328-2338, May 2017.
[31] A. Smolders and H. Visser, "Low side-lobe circularly-polarized phased arrays using a random sequential rotation technique," *IEEE Trans. Antennas Propag.*, vol. 62, no. 12, pp. 6476-6481, Dec. 2014.
[32] J. I. Echeveste, J. Rubio, M. Á. G. de Aza, and C. Craeye, "Pattern synthesis of coupled antenna arrays via element rotation," *IEEE Antennas Wireless Propag. Lett.*, vol. 16, pp. 1707-1710, Feb. 2017.
[33] H. M. Bernety, S. Venkatesh, and D. Schurig, "Analytical phasing of arbitrarily oriented arrays using a fast, analytical far-field calculation method," *IEEE Trans. Antennas Propag.*, vol. 66, no. 6, pp. 2911-2922, Jun. 2018.
[34] R. L. Haupt and D. W. Aten, "Low sidelobe arrays via dipole rotation," *IEEE Trans. Antennas Propag.*, vol. 57, no. 5, pp. 1575-1579, May 2009.
[35] F. Liu, Y. Liu, K. Da Xu, Y.-L. Ban, Q. H. Liu, and Y. J. Guo, "Synthesizing uniform amplitude sparse dipole arrays with shaped patterns by joint optimization of element positions, rotations and phases," *IEEE Trans. Antennas Propag.*, vol. 67, no. 9, pp. 6017-6028, Sep. 2019.
[36] Y. Liu, M. Li, R. L. Haupt, and Y. J. Guo, "Synthesizing shaped power patterns for linear and planar antenna arrays including mutual coupling by refined joint rotation/phase optimization," *IEEE Trans. Antennas Propag.*, vol. 68, no. 6, pp. 4648-4657, Jun. 2020.
[37] Q. Wang, R. Gao, and S. Liu, "Mapping-based optimization method for pattern synthesis via array element rotation," *IEEE Trans. Antennas Propag.*, vol. 68, no. 4, pp. 2736-2742, Apr. 2020.
[38] M. Okoniewski and R. H. Phillion, "Lenses for circular polarization using planar arrays of rotated passive elements," *IEEE Trans. Antennas Propag.*, vol. 59, no. 4, pp. 1217-1227, Apr. 2011.
[39] L. D. Palma, A. Clemente, L. Dussopt, R. Sauleau, P. Potier, and P. Pouliguen, "Circularly-polarized reconfigurable transmitarray in ka-band with beam scanning and polarization switching capabilities," *IEEE Trans. Antennas Propag.*, vol. 65, no. 2, pp. 529-540, Jul. 2017.
[40] Z. H. Jiang, Y. Zhang, J. Xu, Y. Yu, and W. Hong, "Integrated broadband circularly-polarized multi-beam antennas using berry-phase transmit-arrays for ka-band applications," *IEEE Trans. Antennas Propag.*, vol. 68, no. 2, pp. 859-872, Feb. 2020.
[41] P. J. Bevelacqua and C. A. Balanis, "Minimum sidelobe levels for linear arrays," *IEEE Trans. Antennas Propag.*, vol. 55, no. 12, pp. 3442-3449, Dec. 2007.
[42] S. K. Goudos, V. Moysiadou, T. Samaras, K. Siakavara, and J. N. Sahalos, "Application of a comprehensive learning particle swarm optimizer to unequally spaced linear array synthesis with sidelobe level suppression and null control," *IEEE Antennas Wireless Propag. Lett.*, vol. 9, no. 1, pp. 125-129, Mar. 2010.
[43] C. A. Balanis, *Advanced engineering electromagnetics,* 2nd ed. Noboken, NJ, USA: Wiley, 2012.